Instability of viscoelastic curved liquid jets

Alsharif, Abdullah Madhi; Uddin, Jamal; Afzaal, Muhammad F.

DOI:
10.1016/j.apm.2014.12.011

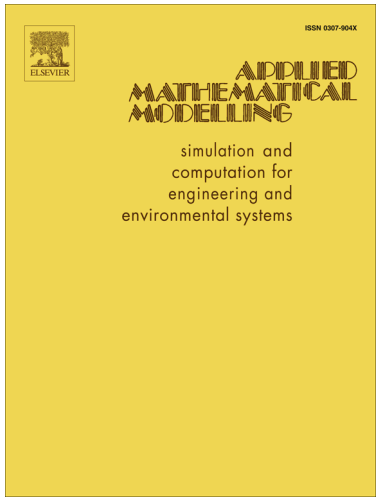

Instability of Viscoelastic Curved Liquid Jets

Abdullah Madhi Alsharif, Jamal Uddin, Muhammad F. Afzaal

PII: S0307-904X(14)00672-6
DOI: http://dx.doi.org/10.1016/j.apm.2014.12.011
Reference: APM 10303

To appear in: *Appl. Math. Modelling*

Please cite this article as: A.M. Alsharif, J. Uddin, M.F. Afzaal, Instability of Viscoelastic Curved Liquid Jets, *Appl. Math. Modelling* (2014), doi: http://dx.doi.org/10.1016/j.apm.2014.12.011

Instability of Viscoelastic Curved Liquid Jets

Abdullah Madhi Alsharif[a,1,*], Jamal Uddin[a], Muhammad F. Afzaal[a],

[a]*School of Mathematics, The University of Birmingham.*
Edgbaston, Birmingham. B15 2TT. UK

Abstract

The industrial prilling process is a common technique to produce small pellets which are generated from the break-up of rotating liquid jets. In many cases the fluids used are molten liquid and/or contain small quantities of polymers and thus typically can be modelled as non-Newtonian liquids. Industrial scale set-ups are costly to run and thus mathematical modelling provides an opportunity to assess methods of improving efficiency and introduces greater levels of precision. In order to understand this process, we will consider a mathematical model to capture the essential physics related to a cylindrical drum, which is rotated about its axis. In this paper, we will model the viscoelastic nature of the fluid using the Oldroyd-B model. An asymptotic approach is used to simplify the governing equations into 1D equations. Moreover, a linear instability analysis is examined and the most unstable modes are found to grow along the jet. Furthermore, the non-linear instability is investigated by using a finite difference scheme to find break-up lengths and droplet formation.

Keywords: Viscoelastic jets, break-up, rotation, non-Newtonian

1. Introduction

Scientists and researchers have investigated phenomena associated with liquid jets, including the process of break-up, drop formation and rupture, because of their relevance to many different industrial applications, such as fertilizer and ink jet printing. A deep understanding of the mechanisms of

*Corresponding author:
Email address: abu.madhi@hotmail.com (Abdullah Madhi Alsharif)

break-up of liquid jets and the associated flow dynamics is heavily dependent on the nature or constitution of the fluid and for this some knowledge of different fluids used in industry are required. The linear instability of incompressible inviscid liquid jets was done by Lord Rayleigh [1] and he found that the instability was caused by surface tension. Rayleigh also found that the most unstable mode of the wavenumber k occurs at $kR = 0.697$ (R is the radius of the jet) with a corresponding wavelength ω of a disturbance $\omega \approx 2\pi R/0.697 \approx 9R$. Weber [2] examined the linear instability of a liquid jet in the presence of the viscosity and he found that the wavelength of most unstable modes is increased by the viscosity. A fuller asymptotic approach has been applied by Papageorgiou [3] on the governing system which describes the evolution of nonlinear waves along the jet. Wallwork *et al.* [4] investigated the linear stability of inviscid liquid jets and they found good agreements between their theoretical and experimental work. The previous work has been examined by Decent *et al.* [5] in the presence of gravity by extending the work of Wallwork [6]. Decent *et al.* [7] also studied the linear stability of spiralling liquid jets by incorporating viscosity and they determined break-up lengths and main and satellite droplet sizes.

Non-Newtonian fluids have been investigated by Uddin *et al.* [8] by using the power-law model to examine the linear instability of a rotating liquid. Uddin *et al.* [8] studied non-linear temporal solutions by using the finite difference scheme based on Lax-Wendroff method for non-Newtonian liquid curved jets. In the same paper they used the simplest model, which is the Power-Law model, for studying non-Newtonian fluids. Renardy [9] found the break-up of Newtonian and non-Newtonian liquid jets by using the Giesekus and Maxwell model. The linear instability of viscoelastic liquid jets has been examined by Middleman [10]. Goldin *et al.* [11] compared the linear stability between inviscid, Newtonian and viscoelastic liquid jets. The Oldroyd-B model has been used by Mageda and Larson [12] to investigate the rheological behaviior for Boger fluids. Schummer and Thelen [13] studied the break-up of a viscoelastic liquid jet by using Jeffrey's model and investigated linear stability.

There is a good article for reviewing the linear and nonlinear instability in viscoelastic flows, which is written by Larson [14]. The beads-on-string structure of viscoelastic jets means that we have large droplets which are connected by thin threads. This phenomenon was examined by Clasen *et al.* [15] using the Oldroyd-B model. The numerical study was conducted by Li and Fontelos [16] for the beads-on-string structure for viscoelastic liquid jets by

using an explicit finite difference method. Fontelos and Li [17] studied the evolution and break-up of viscoelastic liquid jets for two models: the Giesekus model and FENE-P type. The numerical study for pendant drop formation of viscoelastic liquid jets in air which emerged from a nozzle was examined by Davidson *et al.* [18]. The linear stability of viscoelastic fluids has been studied by Renardy [19], where the Weissenberg and Reynolds numbers are large. In addition, the temporal instability of viscoelastic liquid jets moving in an inviscid gas has been discussed by Liu and Liu [20]. Ardekani *et al.* [21] examined the dynamics of beads-on- string structures for weakly viscoelastic liquid jets. Morrison *et al.* [22] examined drop formation of viscoelastic liquid jets emerging from a nozzle.

In this paper, we will extend the work of Decent *et al.* [7] to examine the break-up of rotating viscoelastic liquid jets by using the Oldroyd-B model. To reduce the governing equations into a set of non-dimensional equations, we will apply an asymptotic approach to captures the dynamics of the break-up of low viscosity elastic solutions. We also find steady state solutions and then perform a linear instability analysis on these solutions. Then, we determine the break-up lengths and main and satellite droplet sizes by using a finite difference scheme based on the Lax Wendroff method.

2. Problem Formulation

To model the prilling process, we consider a large cylindrical container having radius s_0 and rotates with angular velocity Ω (see Fig. 1). A small orifice is placed in the side of this container having radius a which is very small compared with the the radius of the container. We examine this problem by considering a coordinate system (X, Y, Z) which rotates with the container and the position of the orifice is at $(s_0, 0, 0)$. The effects of gravity on the jet can be neglected, because we consider the centripetal acceleration of the jet is much greater than the force of gravity. Under this assumption one may assume the jet moves in the (X, Z) plane, so that the centerline can be described by coordinates $(X(s,t), 0, Z(s,t))$, where s is the arc-length along the middle of the jet which emerges from the orifice and t is the time (see Wallower [6]). For this case our governing equations can be written as

$$\boldsymbol{\nabla} \cdot \boldsymbol{u} = 0,$$

$$\rho \left(\frac{\partial \boldsymbol{u}}{\partial t} + \boldsymbol{u} \cdot \boldsymbol{\nabla} \boldsymbol{u} \right) = -\boldsymbol{\nabla} p + \boldsymbol{\nabla} \cdot \boldsymbol{\tau} \, - 2\, \boldsymbol{w} \times \boldsymbol{u} - \boldsymbol{w} \times (\boldsymbol{w} \times \boldsymbol{r}),$$

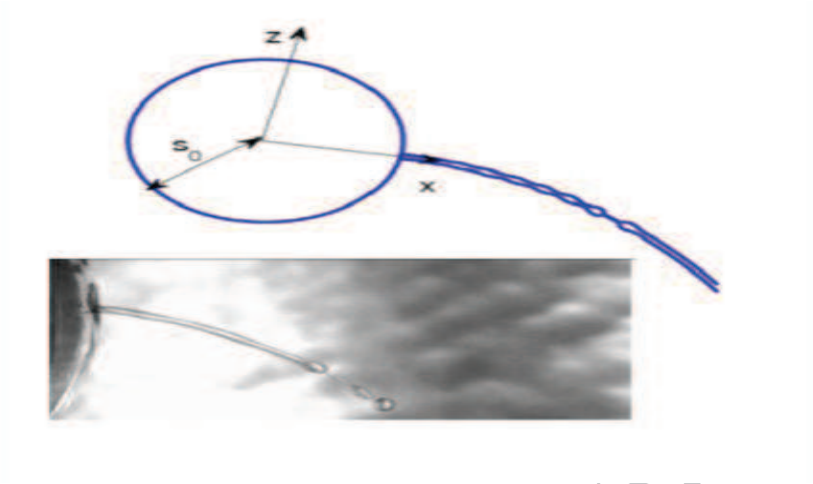

Figure 1: A diagram showing a plan view of rotating cylindrical drum and below a photo taken from Wallwork [6]. The cartesian axes x and z are shown in the figure. The cylindrical drum rotates about its axis with an angular velocity Ω)

$$\boldsymbol{\tau} = \mu_s(\boldsymbol{\nabla u} + (\boldsymbol{\nabla u})^T) + T,$$

$$\frac{\partial T}{\partial t} + (\boldsymbol{u}\cdot\boldsymbol{\nabla})T - T\cdot\boldsymbol{\nabla u} - (\boldsymbol{\nabla u})^T\cdot T = \frac{1}{\lambda}(\mu_p\gamma - T), \tag{1}$$

where $\boldsymbol{u}$ is the velocity in the form $\boldsymbol{u} = u\mathbf{e_s} + v\mathbf{e_n} + w\mathbf{e}_\phi$, ρ is the density of the fluid, p is the pressure, the angular velocity of the container is $\boldsymbol{w} = (0, w, 0)$, μ_s is the viscosity of the solvent, T is the extra stress tensor that represents the elastic contribution to the stresses and μ_p is the viscosity of the polymer. The position of the free surface can be determined by $n - R(s,t,\phi) = 0$, and the normal vector is given by $\nabla(n - R(s,t,\phi))$, which gives

$$\boldsymbol{n} = \frac{1}{E}\left(-\frac{\partial R}{\partial s}\cdot\frac{1}{h_s}\cdot\boldsymbol{e_s} + \boldsymbol{e_n} - \frac{\partial R}{\partial \phi}\cdot\frac{1}{R}\cdot\boldsymbol{e_\phi}\right),$$

where

$$E = \left(1 + \frac{1}{h_s^2}\left(\frac{\partial R}{\partial s}\right)^2 + \frac{1}{R^2}\left(\frac{\partial R}{\partial \phi}\right)^2\right)^{\frac{1}{2}}.$$

The normal stress condition is $\boldsymbol{n}.\boldsymbol{\Pi}.\boldsymbol{n} = \sigma\kappa$, where Π is the total stress tensor given by $-p\boldsymbol{I} + \boldsymbol{\tau}$, σ is the isotropic surface tension and κ is the curvature of the free surface

$$\kappa = \frac{1}{nh_s}\left(-\frac{\partial}{\partial s}\left(\frac{n}{Eh_s}\frac{\partial R}{\partial s}\right) + \frac{\partial}{\partial n}\left(\frac{nh_s}{E}\right) - \frac{\partial}{\partial \phi}\left(\frac{h_s}{En}\frac{\partial R}{\partial \phi}\right)\right).$$

We use the same transformation which is used in Uddin [23] to make our equations dimensionless. Consequently, the momentum equation and the continuity equation are similar to Uddin [23] differing only in the terms of constitutive equations. In summary we use the following scales

$$\bar{u} = \frac{u}{U}\ , \quad \bar{v} = \frac{v}{U}, \quad \bar{w} = \frac{w}{U}, \quad \bar{n} = \frac{n}{a}, \quad \epsilon = \frac{a}{s_0}, \quad \bar{R} = \frac{R}{a},$$
$$\bar{T} = \frac{s_0}{U\mu_0}T, \quad \bar{s} = \frac{s}{s_0}, \quad \bar{t} = \frac{U}{s_0}t, \quad \bar{p} = \frac{p}{\rho U^2}, \quad \bar{X} = \frac{X}{s_0}, \quad \bar{Z} = \frac{Z}{s_0},$$

where u, v and w are the tangential, radial and azimuthal velocity components, U is the exit speed of the jet in the rotating frame, s_0 is the radius of the cylindrical drum, a is the radius of the orifice, ϵ is the aspect ratio of the jet, λ is the relaxation time, T is the extra stress tensor and μ_0 is the total viscosity of the solvent and the polymer; then we will drop the overbars. The governing equations are the same as found in Părău *et al.* [24], but there are extra terms related to viscoelastic terms (for more details see the Appendix).

Where the dimensionless parameters are the Rossby number $Rb = \frac{U}{s_0\Omega}$, the Weber number $We = \frac{\rho U^2 a}{\sigma}$, the Reynolds number $Re = \frac{\rho U a}{\mu_0}$, the Deborah number $De = \frac{\lambda U}{s_0}$ and the ratio between the viscosity of the solvent and the total of the viscosity is $\alpha_s = \frac{\mu_s}{\mu_0} = \frac{\mu_s}{\mu_s + \mu_p}$. Using typical parameter values encountered in prilling (see Wong *et al.* [25]) of $U \sim 0.3 - 1\ ms^{-1}$ and $s_0 \sim 0.04$ m and typical relaxation times of elastic fluids $\lambda \sim 10^{-3} - 10$ (see Entov & Hinch [26]) we can estimate the range of Deborah number values as $De \sim 250 - 0.008$.

3. Non-Dimensionalisation of Boundary Conditions

It can be found that the normal stress condition is

$$p-\frac{2\alpha_s}{Re}\frac{1}{E^2}\Bigg(\epsilon^2\left(\frac{\partial R}{\partial s}\right)^2\frac{1}{h_s^3}\left(\frac{\partial u}{\partial s}+(v\,cos\phi-\sin\phi)(X_sZ_{ss}-Z_sX_{ss})+\frac{h_s}{2\alpha_s}T_{ss}\right)$$
$$+\frac{1}{\epsilon}\frac{\partial v}{\partial n}+\frac{1}{2\alpha_s}T_{nn}+\frac{1}{\epsilon\,R^3}\left(\frac{\partial R}{\partial\phi}\right)^2\left(\frac{\partial w}{\partial\phi}+v+\frac{R}{\alpha_s}T_{\phi\phi}\right)-\frac{\epsilon}{h_s}\frac{\partial R}{\partial s}\Bigg(\frac{1}{h_s}\frac{\partial v}{\partial s}$$
$$+\frac{1}{\epsilon}\frac{\partial u}{\partial n}-\frac{u}{h_s}cos\phi(X_sZ_{ss}-Z_sX_{ss})+\frac{1}{2\alpha_s}T_{sn}\Bigg)+\frac{\epsilon}{Rh_s}\frac{\partial R}{\partial s}\frac{\partial R}{\partial\phi}\Bigg(\frac{1}{\epsilon\,R}\frac{\partial u}{\partial\phi}$$
$$+\frac{u}{h_s}\sin\phi(X_sZ_{ss}-Z_sX_{ss})+\frac{1}{h_s}\frac{\partial u}{\partial s}+\frac{1}{2\alpha_s}T_{s\phi}\Bigg)$$
$$-\frac{1}{R}\frac{\partial R}{\partial\phi}(R\frac{\epsilon\partial w}{\partial n}-\frac{\epsilon w}{R}+\frac{\epsilon}{R}\frac{\partial v}{\partial\phi}\Bigg)=\frac{\sigma\,\kappa}{We}\text{ on }n=R(s,t),\tag{2}$$

where

$$\kappa=\frac{1}{h_s}\left(-\epsilon^2\frac{\partial}{\partial s}\left(\frac{n}{Eh_s}\frac{\partial R}{\partial s}\right)+\frac{\partial}{\partial n}\left(\frac{nh_s}{E}\right)-\frac{\partial}{\partial\phi}\left(\frac{h_s}{En}\frac{\partial R}{\partial\phi}\right)\right).$$

$$E=\left(1+\frac{\epsilon^2}{h_s^2}\left(\frac{\partial R}{\partial s}\right)^2+\frac{1}{R^2}\left(\frac{\partial R}{\partial\phi}\right)^2\right)^{\frac{1}{2}}.$$

$$h_s=1+\epsilon n\cos\phi(X_sZ_{ss}-X_{ss}Z_s).$$

The first tangential stress condition is

$$\left(1-\epsilon^2\left(\frac{\partial R}{\partial s}\right)^2\frac{1}{h_s^2}\right)\left\{\epsilon\frac{\partial v}{\partial s}+h_s\frac{\partial u}{\partial n}-\epsilon u\cos\phi(Z_sZ_{ss}-X_{ss}Z_s)+\frac{\epsilon}{\alpha_s}T_{sn}\right\}+2\epsilon\frac{\partial R}{\partial s}$$
$$\left\{\frac{\partial v}{\partial n}-\epsilon\frac{\partial u}{\partial s}\frac{1}{h_s}-\frac{\epsilon}{h_s}v\cos\phi-w\sin\phi(X_sZ_{ss}-X_{ss}Z_s)-\frac{\epsilon}{2\alpha_s}(T_{ss}-T_{nn})\right\}=0,\tag{3}$$

and the second tangential stress condition is

$$\left(1-\left(\frac{\partial R}{\partial\phi}\right)^2\frac{1}{R^2}\right)\left(\frac{\partial w}{\partial n}-\frac{w}{R}+\frac{1}{R}\frac{\partial v}{\partial\phi}+\frac{\epsilon}{\alpha_s}T_{n\phi}\right)+$$
$$\frac{2}{R}\frac{\partial R}{\partial\phi}\left(\frac{\partial v}{\partial n}-\frac{1}{R}\left(\frac{\partial w}{\partial\phi}+v\right)+\frac{\epsilon}{\alpha_s}(T_{nn}-T_{\phi\phi})\right)=0.\tag{4}$$

Another boundary condition is the arc-length condition $X_s^2 + Z_s^2 = 1$. The kinematic condition is

$$h_s \left(\epsilon \frac{\partial R}{\partial t} + (\cos\phi + \frac{1}{n}\frac{\partial R}{\partial t}\sin\phi(X_t Z_s - X_s Z_t) - v + \frac{\partial R}{\partial \phi}\frac{w}{n} \right)$$
$$+\epsilon u \frac{\partial R}{\partial s} - \epsilon \frac{\partial R}{\partial s}(X_t Z_s - X_s Z_t + \epsilon n \cos\phi(X_s Z_{ss} - Z_s X_{ss})) = 0. \quad (5)$$

4. Asymptotic Analysis

u, v, w and p in Taylor's series are expanded in ϵn (see Eggers [27] and Hohman *et al.* [28]) and $R, X, Z, T_{ss}, T_{nn}, T_{\phi\phi}$ in asymptotic series in ϵ. We suppose that the leading order of the axial component of the velocity is independent of ϕ. It is also assumed that small perturbations do not affect the centerline. Therefore, we have

$$\begin{aligned}
&(u, v, w)(s, n, \phi, t) = (u_0, 0, 0)(s, t) + (\epsilon\, n)(u_1, v_1, w_1)(s, \phi, t) + ... \\
&p(s, n, \phi, t) = p_0(s, \phi, t) + (\epsilon\, n)p_1(s, \phi, t) + ... \\
&R(s, n, \phi, t) = R_0(s, t) + (\epsilon)R_1(s, \phi, t) + ... \\
&(X, Z)(s, n, \phi, t) = (X_0, Z_0)(s) + (\epsilon)(X_1, Z_1)(s, t) + ... \\
&(T_{ss}, T_{nn}, T_{\phi\phi})(s, n, \phi, t) = (T^0_{ss}, T^0_{nn}, 0)(s, t) + \epsilon\,(T^1_{ss}, T^1_{nn}, T^1_{\phi\phi})(s, t) + ... \\
&(T_{sn}, T_{s\phi}, T_{n\phi})(s, n, \phi, t) = \epsilon\,(T^1_{ss}, T^1_{nn}, \epsilon T^1_{\phi\phi})(s, t) + ... \quad (6)
\end{aligned}$$

It can be found from the continuity equation that

$$O(\epsilon n): \quad u_{0s} + 2v_1 + w_{1\phi} = 0, \quad (7)$$
$$O(\epsilon n)^2: \quad u_{1s} + 3v_2 + w_{2\phi} + 3v_1 + (w_{1\phi}\cos\phi - w_1\sin\phi)$$
$$(X_s Z_{ss} - X_{ss} Z_s) = 0. \quad (8)$$

By solving the second tangential stress condition, we can see that

$$O(\epsilon n): \quad R_0^3 v_{1\phi} = 0, \quad (9)$$
$$O(\epsilon n)^2: \quad 3R_0^2 R_1 v_{1\phi} + R_0^4(w_2 + v_{2\phi}) - 2R_0^2 R_{1\phi} w_{1\phi} = 0. \quad (10)$$

It can be seen that $v_{1\phi} = 0$, and by differentiating (7), we obtain $w_{1\phi\phi} = 0$. Because w_1 is periodic in ϕ we must have $w_1 = w_1(s, t)$. That leads to $v_1 = -\frac{u_{0s}}{2}$ and from (10) we obtain

$$w_2 + v_{2\phi} = 0. \quad (11)$$

Using the first tangential stress condition, it can be obtained that

$$O(\epsilon n): \quad u_1 = u_0 \cos\phi (X_s Z_{ss} - X_{ss} Z_s), \tag{12}$$

$$O(\epsilon n)^2: \quad u_2 = \frac{3}{2} u_{0s} \frac{R_{0s}}{R_0} + \frac{u_{0ss}}{4} + \frac{R_{0s}}{2\alpha_s R_0}(T^0_{ss} - T^0_{nn}). \tag{13}$$

By differentiating (11) with respect to ϕ we have

$$w_{2\phi} = -v_{2\phi\phi}, \tag{14}$$

so that

$$v_{2\phi\phi} - 3v_2 = u_{1s} + (3v_1 \cos\phi - w_1 \sin\phi)(X_s Z_{ss} - X_{ss} Z_s), \tag{15}$$

so when the expression for u_1 and v_1 are used, we obtain

$$v_{2\phi\phi} - 3v_2 = \left(u_0(X_s Z_{sss} - X_{sss} Z_s) - \frac{u_{0s}}{2}(X_s Z_{ss} - X_{ss} Z_s)\right) \cos\phi$$
$$-w_1 \sin\phi (X_s Z_{ss} - X_{ss} Z_s). \tag{16}$$

v_2 and w_2 are periodic solutions

$$v_2 = \frac{1}{4}\left(\frac{u_{0s}}{2}(X_s Z_{ss} - X_{ss} Z_s) - u_0(X_s Z_{sss} - X_{sss} Z_s)\right) \cos\phi +$$
$$\frac{w_1}{4} \sin\phi (X_s Z_{ss} - X_{ss} Z_s), \tag{17}$$

$$w_2 = \frac{1}{4}\left(\frac{u_{0s}}{2}(X_s Z_{ss} - X_{ss} Z_s) - u_0(X_s Z_{sss} - X_{sss} Z_s)\right) \sin\phi +$$
$$\frac{w_1}{4} \cos\phi (X_s Z_{ss} - X_{ss} Z_s). \tag{18}$$

Based on the momentum equation in the radial direction, we have at leading order $p_{0n} = 0$ and at order ϵ

$$p_1 = \left(u_0^2(X_s Z_{ss} - X_{ss} Z_s) - \frac{2}{Rb} u_0 + \frac{(X_0 + 1)Z_{0s} - Z_0 X_{0s}}{Rb^2}\right) \cos\phi$$
$$-\frac{\alpha_s}{Re}\left(\frac{5}{2} u_{0s}(X_s Z_{ss} - X_{ss} Z_s) + u_{0s}(X_s Z_{sss} - X_{sss} Z_s)\right) \cos\phi +$$
$$\frac{\alpha_s}{Re} w_1 \sin\phi (X_s Z_{ss} - X_{ss} Z_s). \tag{19}$$

We will use X and Z instead of X_0 and Z_0 for simplicity. For the momentum equation in the azimuthal direction, we have at leading order, $p_{0\phi} = 0$. At

the next order, which is order ϵ, we obtain the equation given above. From the normal stress condition at the leading order, we have

$$p_0 = -\frac{\alpha_s u_{0s}}{Re} + \frac{1}{R_0 We} + \frac{T^0_{nn}}{Re}, \tag{20}$$

and we also have at order ϵ

$$p_1 = \frac{1}{R_0 We}\left(-\frac{R_{1\phi\phi}+R_1}{R_0^2} + \cos\phi(X_s Z_{ss} - X_{ss} Z_s)\right) + \frac{4\alpha_s v_2}{Re}. \tag{21}$$

By substituting the expression for v_2, we obtain

$$\begin{aligned} p_1 = {} & \frac{1}{R_0 We}\left(-\frac{R_{1\phi\phi}+R_1}{R_0^2} + \cos\phi(X_s Z_{ss} - X_{ss} Z_s)\right) + \\ & \frac{\alpha_s}{Re}\left(\frac{u_{0s}}{2}(X_s Z_{ss} - X_{ss} Z_s) - u_0(X_s Z_{sss} - X_{sss} Z_s)\right)\cos\phi + \\ & \frac{\alpha_s w_1}{Re}\sin\phi(X_s Z_{ss} - X_{ss} Z_s). \end{aligned} \tag{22}$$

If we substitute p_1 from (19) in the previous equation, we obtain

$$(X_s Z_{ss} - X_{ss} Z_s)\left(u_0^2 - \frac{3\alpha_s}{Re}u_{0s} - \frac{1}{We R_0}\right) - \frac{2}{Rb}u_0 + \frac{(X+1)Z_s - Z X_s}{Rb^2} = 0. \tag{23}$$

The Navier-Stokes equation in the axial direction at order ϵ is

$$\begin{aligned} u_{0t} + u_0 u_{0s} = {} & -p_{0s} + \frac{(X+1)X_s + Z Z_s}{Rb^2} + \\ & \frac{\alpha_s}{Re}(u_{oss} + 4u_2 + u_{2\phi\phi}) + \frac{1}{Re}\frac{\partial T^0_{ss}}{\partial s}. \end{aligned} \tag{24}$$

After substituting the expressions for u_2 and p_0, the previous equation becomes

$$\begin{aligned} u_{0t} + u_0 u_{0s} = {} & -\frac{1}{We}\frac{\partial}{\partial s}\left(\frac{1}{R_0}\right) + \frac{(X+1)X_s + Z Z_s}{Rb^2} \\ & + \frac{3\alpha_s}{Re}\left(u_{0ss} + 2u_{0s}\frac{R_{0s}}{R}\right) + \frac{1}{Re}\left(\frac{1}{R_0^2}\frac{\partial}{\partial s}R_0^2\,(T^0_{ss} - T^0_{nn})\right). \end{aligned} \tag{25}$$

From the kinematic condition at order ϵ, it can be obtained

$$R_{0t} + \frac{u_{0s}}{2}R_0 + u_0 R_{0s} = 0. \tag{26}$$

From the extra stress tensor, we have at leading order as follows

$$\frac{\partial T^0_{ss}}{\partial t} + u_0 \frac{\partial T^0_{ss}}{\partial s} - 2\frac{\partial u_0}{\partial s} T^0_{ss} = \frac{1}{De}\left(2(1-\alpha_s)\frac{\partial u_0}{\partial s} - T^0_{ss}\right), \quad (27)$$

$$\frac{\partial T^0_{nn}}{\partial t} + u_0 \frac{\partial T^0_{nn}}{\partial s} + \frac{\partial u_0}{\partial s} T^0_{nn} = -\frac{1}{De}\left((1-\alpha_s)\frac{\partial u_0}{\partial s} + T^0_{nn}\right). \quad (28)$$

We have the last equation, which is the arc-length at order ϵ

$$X_s^2 + Z_s^2 = 1. \quad (29)$$

5. Steady State Solutions

From (26) $R_0^2 u_0 = constant$ is found. Now we use the initial conditions $R(0) = 1$ and $u(0) = 1$, so that we obtain $R_0^2 u_0 = 1$ after using this expression. Equations (25) and (23) become

$$u_0 u_{0s} = -\frac{1}{2We}\frac{u_{0s}}{\sqrt{u}} + \frac{(X+1)X_s + ZZ_s}{Rb^2} + \frac{3\alpha_s}{Re}\left(u_{0ss} - \frac{u_{0s}^2}{u_0}\right) + \frac{1}{Re}\left(\frac{\partial}{\partial s}(T^0_{ss} - T^0_{nn}) - \frac{u_{0s}}{u_0}(T^0_{ss} - T^0_{nn})\right), \quad (30)$$

$$(X_s Z_{ss} - X_{ss} Z_s)\left(u_0^2 - \frac{3\alpha_s}{Re}u_{0s} - \frac{\sqrt{u}}{We}\right) - \frac{2}{Rb}u_0 + \frac{(X+1)Z_s - ZX_s}{Rb^2} = 0, \quad (31)$$

$$u_0 \frac{\partial T^0_{ss}}{\partial s} - 2\frac{\partial u_0}{\partial s} T^0_{ss} = \frac{1}{De}\left(2(1-\alpha_s)\frac{\partial u_0}{\partial s} - T^0_{ss}\right), \quad (32)$$

$$u_0 \frac{\partial T^0_{nn}}{\partial s} + \frac{\partial u_0}{\partial s} T^0_{nn} = -\frac{1}{De}\left((1-\alpha_s)\frac{\partial u_0}{\partial s} + T^0_{nn}\right), \quad (33)$$

$$X_s^2 + Z_s^2 = 1. \quad (34)$$

If we allow $De \to 0$ and $\alpha_s = 1$ (which implies $\mu_p = 0$) we have T^0_{ss} & $T^0_{nn} \to 0$ and (30)-(34) which produce the equivalent set of equations found in Părău

et al. [29, 24]. Furthermore, if we let $Re \to \infty$ we obtain the inviscid equation of Decent *et al*. [5]. In the equations (30)-(34), we have five unknowns, which are X, Z, u_0, T^0_{ss} and T^0_{nn}. We solve these equations for high viscosity fluids by using the Runge-Kutta method. Părău *et al*. [29, 24] have used the Runge-Kutta method and Newton's method to solve the problem of viscous liquid curved jets and compared the results with the Runge-Kutta method for inviscid case. They found a good agreement between the two methods for the steady centerline and radius of the jet. Părău *et al*. [29, 24] also found that there is a very little difference with and without viscosity in numerical solutions. To find the steady state solutions for the equations (30)-(34), we make $Re \to \infty$ in the inviscid case, because we consider low viscosity fluids here. Decent *et al*. [7] solved the Newtonian fluid by using this assumption. Therefore, we will use the same assumption in this paper to find the steady state solutions. However, if we consider that these equations are independent of t, this means that $X_{0t} \neq 0$ and $Z_{0t} \neq 0$. This assumption leads to there being some extra unsteady terms in these equations in $E = Z_s X_s - Z_t X_s$. (see Părău *et al*. [24]). Părău *et al*. [24] have used that $X(s,t) = X_0(s,t) + \hat{X}(s,t)$ and $Z(s,t) = Z_0(s,t) + \hat{Z}(s,t)$ and then found the linearized in $\hat{X}$ and $\hat{Z}$. Parau *et al*. [24] also found the maximum deviation of order 10^{-2} of the perturbation of the steady state centerline. This value is very small compared to the $O(1)$ values of $X_0(s)$ and $Z_0(s)$. Therefore, $E \approx 0$ is a very accurate assumption to be taken from the orifice to the break-up point. Experimentally Wong *et al*. [25] observed that the centerline of the jet is steady, which means $X_{st} \approx 0$, $Z_{st} \approx 0$ and $E \approx 0$. As we mentioned earlier, we solve the equations (30)-(34) for inviscid centerline problem (which means $Re \to \infty$) using the Runge-Kutta method with the boundary conditions at the nozzle as $X(0) = Z(0) = Z_s(0) = T^0_{ss}(0) = T^0_{nn}(0) = 0$ and $u(0) = X_s(0) = 1$. In Figs. 2 and 3, we find the jet trajectory, the extra stress tensor (T^0_{ss}, T^0_{nn}) and the jet radius for different values of the Rossby number by using the Runge-Kutta method. In the next paragraph, we will give more explanations about these figures. For different values of the Rossby number (rotation rates), we plot a graph (Fig. 2) to see the effect of this number on the liquid jet. This graph shows that when the Rossby number is small, the liquid coils quickly. From this figure, it can be seen that the jet becomes thin when the arc-length is increased. In addition, in Fig. 3 we display the relationship between the extra stress tensor, which is T^0_{ss}, and the arc-length for different values of the Rossby number and this graph shows that when the rotation is very high the extra stress tensor has more effect on the jet. Moreover, these graphs cor-

respond to different values of the Rossby number for the extra stress tensor T^0_{nn} and the radius of the jet R_0 along the arc-length s.

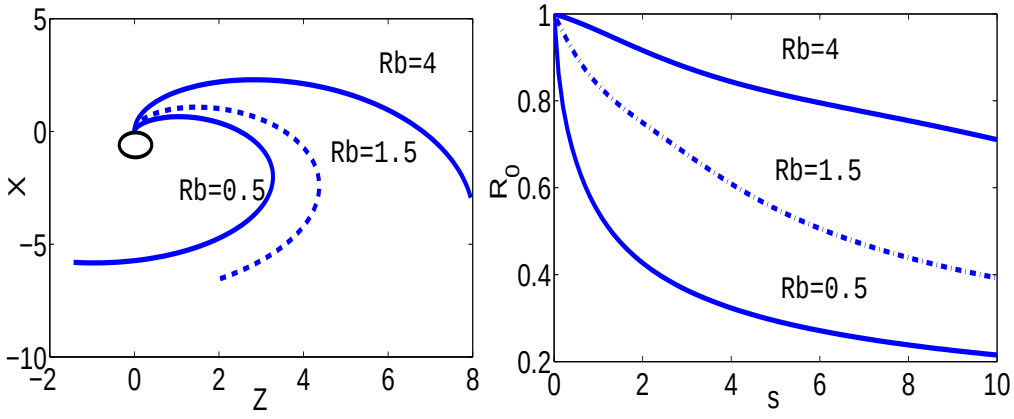

Figure 2: The trajectory of an inviscid liquid jet and the radius of rotating liquid jets, which is solved by using a Runge-Kutta method and emerging from an orifice placed at (0,0). The jet curves increase when the Rossby number increases (rotation rates). We use $We = 10, De = 10, \alpha_s = 0.2$.

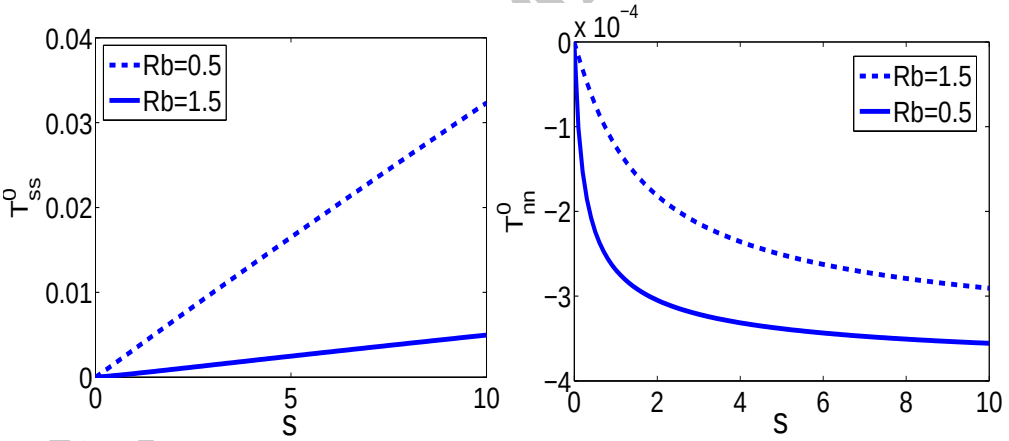

Figure 3: Graph showing the relationship between T^0_{ss} , T^0_{nn} and arc-length s of rotating liquid jets for different values of Rossby number at $We = 10, De = 10, \alpha_s = 0.2$.

6. Temporal Instability

Now we make small perturbations by considering small travelling wave modes about the steady state solutions (30)-(34) which are obtained from the previous section. So that we have

$$(u, R, T_{ss}, T_{nn}) = (u_0, R_0, T_{0ss}, T_{0nn}) + \delta(\hat{u}, \hat{R}, \hat{T}_{ss}, \hat{T}_{nn})\, exp(i\kappa\bar{s} + \omega\bar{t}), \quad (35)$$

where $\bar{s} = s/\epsilon$ is small length scales, $\bar{t} = t/\epsilon$ is small time scales, $k = k(s)$ and $\omega = \omega(s)$ are the wavenumber and frequency of the disturbances, and δ is a small constant which is $0 < \delta < \epsilon^2$ (see Uddin [23]). The symbols with subscripts denote steady state solutions. In order to prevent instability of wave modes with zero wavelength, we replace the leading order pressure term in equation (25) with the full curvature expression (see Eggers [27]).

$$u_{0t} + u_0 u_{0s} = -\frac{1}{We}\left(\frac{1}{R_0(1+R_{0s}^2)^{1/2}} - \frac{\epsilon^2 R_{0ss}}{(1+R_{0s}^2)^{3/2}}\right)_s + \frac{(X+1)X_s + ZZ_s}{Rb^2}$$
$$+\frac{3\alpha_s}{Re}\left(u_{0ss} + 2u_s\frac{R_s}{R}\right) + \frac{1}{Re}\left(\frac{\partial}{\partial s}(T_{ss}^0 - T_{nn}^0) - \frac{u_{0s}}{u_0}(T_{ss}^0 - T_{nn}^0)\right). \quad (36)$$

The perturbation equations (35) are now substituted into the equations (26)-(28) and (36), then we obtain the eigenvalue relation at leading order which has the form

$$\left(\omega + iku_0\right)^2 + \tfrac{3\tilde{\alpha_s}k^2}{Re}\left(\omega + iku_0\right) - \tfrac{k^2R_0}{2We}\left(\left(\tfrac{1}{R_0^2} - k^2\right) - \tfrac{2We}{R_0\,Re}(T_{ss}^0 - T_{nn}^0)\right) -$$
$$\tfrac{k^2}{Re}\left(2T_{ss}^0 + T_{nn}^0 + \tfrac{3}{De}\right) = 0. \quad (37)$$

There is a new scaling for the viscosity ratio which is $\tilde{\alpha_s} = \frac{\alpha_s}{\epsilon}$. Without this new scaling, we cannot bring the viscous term into the equations which derived the dispersion relation. We mentioned earlier, $\alpha_s + \alpha_p = 1$, where α_s and α_p are the solvent viscosity and the polymeric viscosity respectively. After substituting the new scaling, the last equation becomes $\epsilon\tilde{\alpha_s} + \alpha_p = 1$, which means that $\alpha_p \gg \alpha_s$. However, both the solvent viscosity and the polymeric viscosity are very small $\mu_s, \mu_p \ll 1$. By choosing $\omega_i = -ku_0$, we get

$$\omega_r^2 + \frac{3\tilde{\alpha_s}k^2}{Re}\omega_r - \frac{k^2R_0}{2We}\left((\frac{1}{R_0^2} - k^2) - \frac{2We}{R_0\,Re}(T_{ss}^0 - T_{nn}^0)\right) - \frac{k^2}{Re}\left(2T_{ss}^0 + T_{nn}^0 + \frac{3}{De}\right) = 0, \quad (38)$$

which becomes

$$\omega_r = \frac{-3\tilde{\alpha}_s k^2}{2Re} + \frac{k}{2}\sqrt{\frac{2}{R_0 We}\Big((1-(kR_0)^2 - \frac{2We}{R_0\, Re}B\Big) + \frac{4}{Re}\Big(2T^0_{ss} + T^0_{nn} + \frac{3}{De}\Big) + \Big(\frac{3\tilde{\alpha}_s k}{Re}\Big)^2}. \quad (39)$$

We differentiate the last equation with respect to k to find the most unstable wavenumber $k = k^*$ which is given by

$$k^* = \frac{1}{(2R_0^3)^{1/4}} \frac{\Big(\frac{R_0 GWe}{2} + 1 - 2B\Big)^{\frac{1}{2}}}{\sqrt{\Big(3\tilde{\alpha}_s Oh + \sqrt{2R_0}\Big)}}, \quad (40)$$

where $B = T^0_{ss} - T^0_{nn}$ and $G = \frac{4}{Re}\Big(2T^0_{ss} + T^0_{nn} + \frac{3}{De}\Big)$. For temporal instability, the growth rate ω_r is positive which occurs when $0 < kR_0 < 1$. When $De = 0$ and $T^0_{ss} = T^0_{nn} = 0$ the dispersion relation is

$$k^* = \frac{1}{(2R_0^3)^{1/4}} \frac{1}{\sqrt{\Big(3Oh + \sqrt{2R_0}\Big)}}, \quad (41)$$

which is the same as for Newtonian liquid jets which was found by Decent *et al*. [7]. The relationship between the growth rate and the wavenumber is plotted in Fig. 4 for three fluids, which are inviscid fluid, viscous fluid and viscoelastic fluid. It can be observed from this graph that viscoelastic jets are more unstable than Newtonian jets and less unstable than inviscid jets. We also plot a graph between the growth rate and the wavenumber for various values of s (see Fig. 5). It can be seen from this figure that the most unstable wavenumber k increases which means that wavenumber disturbances become short. In Fig. 6, we chose different values of the Rossby number, $Rb = 0.5, 1.5$ and 4, where the Reynolds number is $Re = 6$ for obtaining the relationship between the growth rate of the most unstable mode and the arc-length s. From this figure, it can be noticed that when the Rossby number is small (meaning the rotation is high), the growth rate of the most unstable mode becomes large. Fig. 7 shows the relationship between the maximum wave number for the most unstable k^* and the arc-length s for different values of the Rossby number, Rb, and found that the rotation increases the maximum wavenumber.

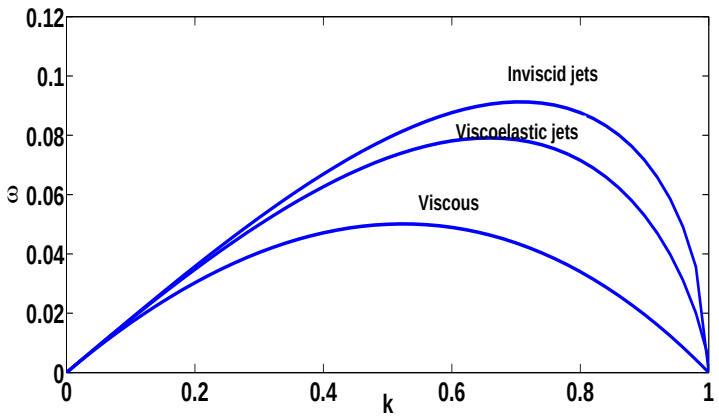

Figure 4: Graph showing the relationship between the growth rate against the wavenumber for three fluids, which are inviscid fluid where $We = 15$, viscoelastic fluid where $Oh = 0.003, We = 15, \tilde{\alpha_s} = 20$ and viscous fluid at $Oh = 0.003, We = 15$.

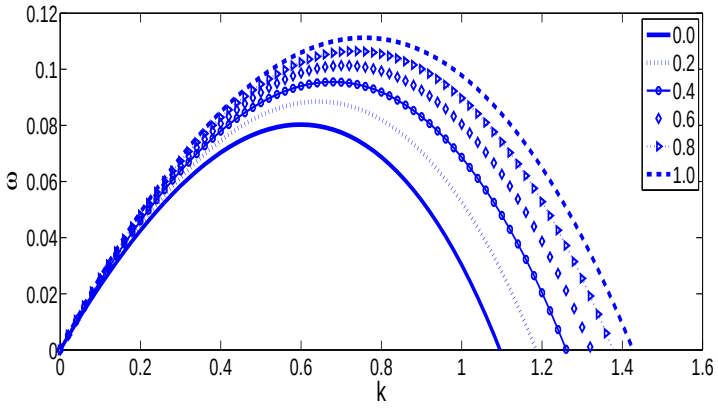

Figure 5: Graph showing the relationship between the growth rate against the wavenumber for various values of s at $Oh = 0.003, De = 15, \tilde{\alpha_s} = 20$.

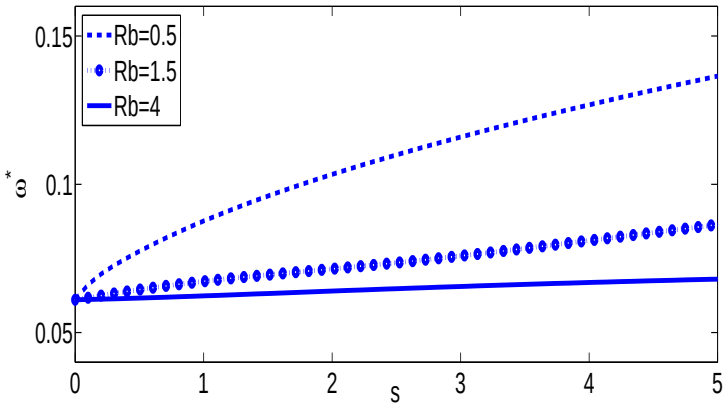

Figure 6: Graph showing the relationship between the growth rate ω_r^* for the most unstable mode and the arc-length s for a viscoelastic liquid jet for different values of the Rossby number Rb, where the dimensionless numbers are $Oh = 0.003$, $De = 15$, $\tilde{\alpha_s} = 20$.

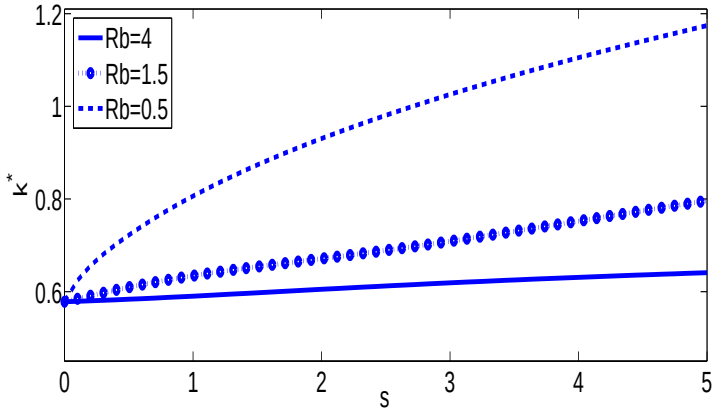

Figure 7: Graph showing the relationship between the wavenumber of the most unstable k^* and the arc-length s for a viscoelastic liquid jet for different values of the Rossby number Rb, where the dimensionless numbers are $Oh = 0.003, De = 15, \tilde{\alpha_s} = 20$.

7. Nonlinear Temporal Solutions

Linear instability analysis predicts that liquid jets break up and produce uniform drop sizes along the axis of approximately the same wavelength of initial disturbances. However, it can be observed that a number of smaller satellite droplets appeared in this case which are not equal in size. Therefore, we use nonlinear temporal analysis to examine the break-up length and the formation of satellite droplets. We replace the leading order pressure term $p_0 = \frac{1}{We}\frac{1}{R_0}$ in the equation (25) with the expression for the full curvature term which contains only R_0 and is not ϕ-dependent, namely

$$p = \frac{1}{We}\left[\frac{1}{R_0(1+\epsilon^2 R_{0s}^2)^{1/2}} - \frac{\epsilon^2 R_{0ss}}{(1+\epsilon^2 R_{0s}^2)^{3/2}}\right]. \tag{42}$$

For simplicity, We denote $A = A(s,t)$, where $A(s,t) = R^2(s,t)$, and then we rewrite our equations (25)-(28) as

$$\frac{\partial u}{\partial t} = -\Big(\frac{u^2}{2}\Big)_s - \frac{1}{We}\frac{\partial}{\partial s}\frac{4\Big(2A + (\epsilon A_s)^2 - \epsilon^2 A A_{ss}\Big)}{\Big(4A + (\epsilon A_s)^2\Big)^{3/2}} + \frac{(X+1)X_s + ZZ_s}{Rb^2} + \frac{3\alpha_s}{Re}\frac{(Au_s)_s}{A} + \frac{1}{Re}\frac{\Big(A(T_{ss} - T_{nn})\Big)_s}{A}, \tag{43}$$

$$\frac{\partial A}{\partial t} = -\frac{\partial}{\partial s}(Au), \tag{44}$$

$$\frac{\partial T_{ss}}{\partial t} = -\frac{\partial}{\partial s}(uT_{ss}) + 3\frac{\partial u}{\partial s}T_{ss} + \frac{1}{De}\Big(2(1-\alpha_s)\frac{\partial u}{\partial s} - T_{ss}\Big), \tag{45}$$

$$\frac{\partial T_{nn}}{\partial t} = -\frac{\partial}{\partial s}(uT_{nn}) - \frac{1}{De}\Big((1-\alpha_s)\frac{\partial u}{\partial s} + T_{nn}\Big). \tag{46}$$

We solve this system of equations as we did in section 5 for the steady state by using the initial conditions at $t = 0$ which are $A(s, t = 0) = R_0^2(s)$, $u(s, t = 0) = u_0(s), T_{ss}(s, t = 0) = 0$, $T_{nn}(s, t = 0) = 0$. At the nozzle, we use upstream boundary conditions

$$A(0,t) = 1,\ u(0,t) = 1 + \delta \sin\left(\frac{\kappa t}{\epsilon}\right),$$

where κ is a non-dimensional wavenumber of the perturbation of frequency and δ is the amplitude of the initial non-dimensional velocity disturbance of which we used a small size. In the calculation, we have used the value of $\epsilon(=\frac{a}{s_0})$ which can be measured from experiments using $\epsilon = 0.01$. This value is the same as that found in experiments and the industrial problem (see Wong *et al*. [25]). We investigate the break-up length, the main and the satellite droplet size for viscoelastic liquid curved jets by using a second order finite difference scheme which is known as the two-step Lax-Wendroff method. The break-up is chosen to occur when the radius is less than 5% for consistency with earlier work (see Părău *et al*. [24]). In this simulation, the jet profile and the radius are plotted in Fig. 8 for two different values of the Rossby number ($Rb = 1$ and 8). It can be seen that the rotation rate has increased the break up length of the jet. In Fig. 9, we studied the effect of the rotation rate on the break up length and found that decreasing rotation rates decrease the break-up length. This result agrees with the case of Newtonian liquid curved jets (see Părău *et al*. [24]). In Figs. 10 and 11, it can be noticed that when the viscosity ratio increases, the break-up length and the break-up time also increase. Fig. 12 shows the effects of the viscosity ratio on the droplet radius for the main and satellite droplet sizes. We found that this viscosity ratio has a small effect on the main droplet size. However, the influence can be seen in the satellite droplet size. As the viscosity ratio increases, the satellite droplet size also increases. Fig. 13 shows the main and satellite droplet size for viscoelastic liquid curved jets. We can see that the main droplet size does not change too much with increasing rotation rates, whereas the satellite droplet size decreases and this result agrees with the Newtonian spiralling jets. In addition, when we increase the Deborah number the break-up length increases and the main and satellite droplets increase as well which are plotted in Figs 14 and 15. In Fig. 16, we show the difference between three types of liquids (inviscid, viscous and viscoelastic) for the radius of the jet and the arc-length s. It can be observed from this figure that the break-up of viscoelastic liquid jets happens faster than viscous liquid jets and slower than inviscid liquid jets. Părău *et al*. [24] plot a graph to show the relationship between the radius of the jet and the arc-length for two liquids, inviscid and viscous. They found that the inviscid jets break up faster than the Newtonian jet.

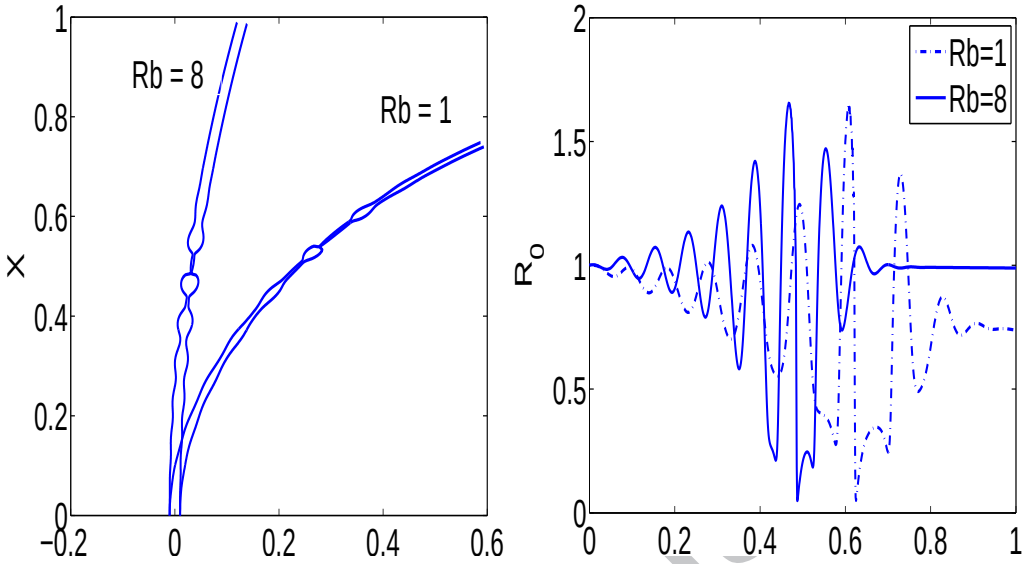

Figure 8: The profile of two different values of the Rossby number, where the values of the parameters are $Re = 1000, We = 10, De = 10, k = 0.8, \alpha_s = 0.2, \delta = 0.01$. We can see that when we increase the rotation rate, the break-up length also increases.

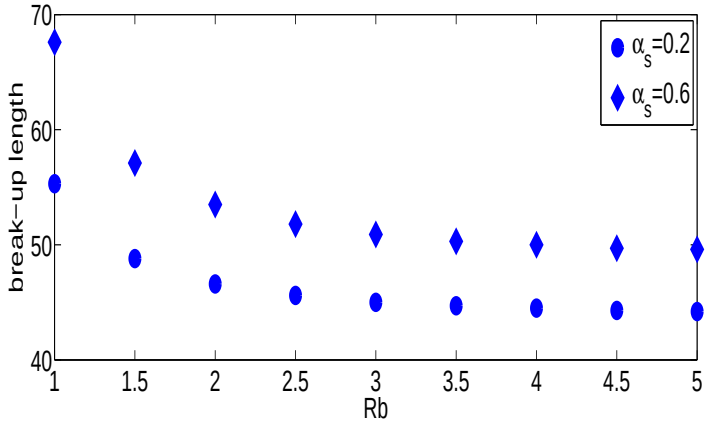

Figure 9: Graph showing the relationship between the break up length and Rb. Where $Re = 3000, We = 10, De = 10, k = 0.5, \delta = 0.01$ and $\alpha_s = 0.2$. We can see that the break-up length increases, when the rotation rate is increased.

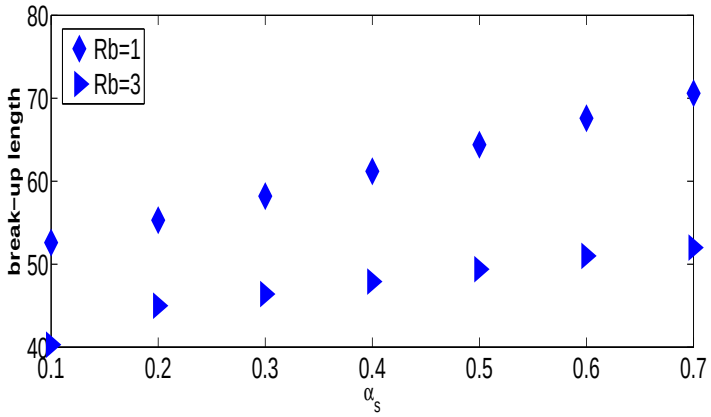

Figure 10: The break up length of viscoelastic liquid jets plotted against the ratio of viscosity for two values of $Rb = 1$ an 3. The parameters are $Re = 3000, We = 10, De = 10, k = 0.5$ and $\delta = 0.01$. We observe that when we increase the ratio of the viscosity, the break-up increases for high rotation rates.

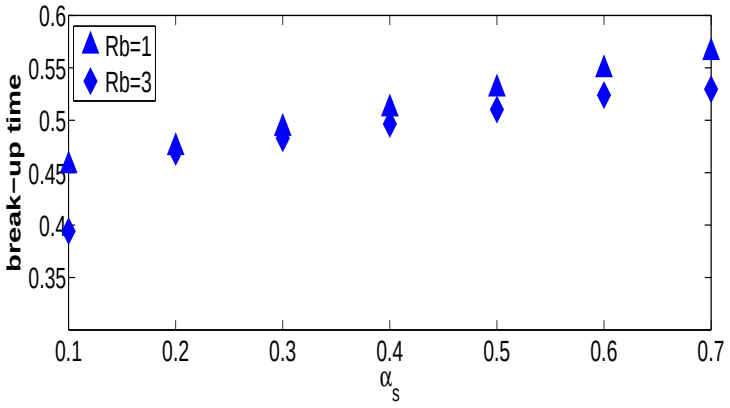

Figure 11: Graph showing the relationship between the main and satellite droplet radius of the jet and the viscosity ratio, α_s. We can observe that the satellite droplet radius increases with an increased viscosity ratio. We use $Re = 3000, We = 10, De = 10, k = 0.5, \delta = 0.01, \alpha_s = 0.2$ and $Rb = 1$.

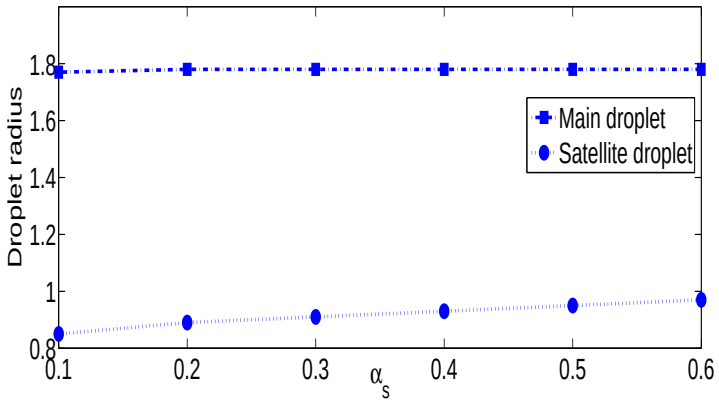

Figure 12: Graph showing the relationship between the radius of the jet and the arc-length for three different liquids. We can see that satellite droplets increase with increasing the viscosity ratio. We use $Re = 1000, We = 10, De = 10, k = 0.6$ and $Rb = 1$.

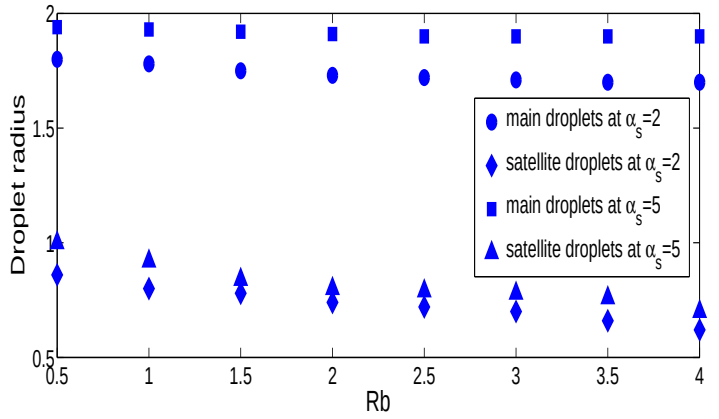

Figure 13: Graph showing the relationship between the radius of the jet and the Rossby number for two different values of the ratio of the viscosity. We can notice that satellite droplets increase with increasing ratio rates. We use $Re = 1000, We = 10, De = 10, k = 0.6, \alpha_s = 0.2, \delta = 0.01$ and $Rb = 1$.

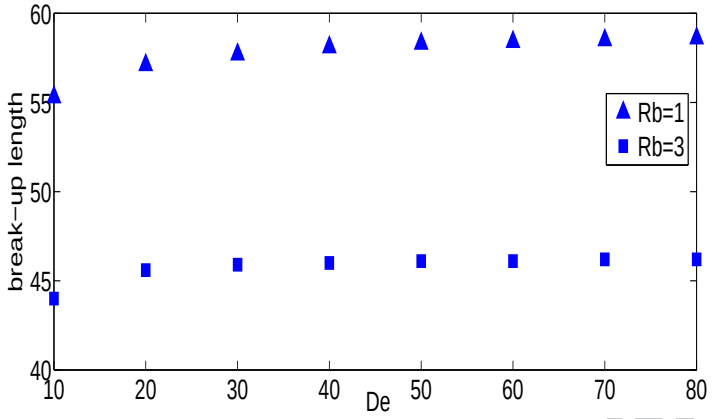

Figure 14: Graph showing the break-up versus the Deborah number for two values of the Rossby number. It can be observed that when we decrease the Deborah number the break-up decreases. We use $Re = 3000, We = 10, \delta = 0.01, k = 0.5, \alpha_s = 0.2$.

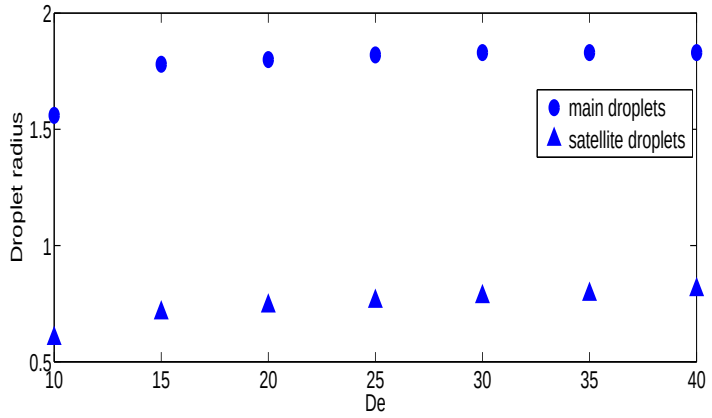

Figure 15: Graph showing the relationship between the radius of the jet and the Deborah number. It can be seen that the main and satellite droplets are increased when the Deborah number is decreased. We use $Re = 1000, We = 10, k = 0.5, \delta = 0.01, \alpha_s = 0.2$ and $Rb = 1$.

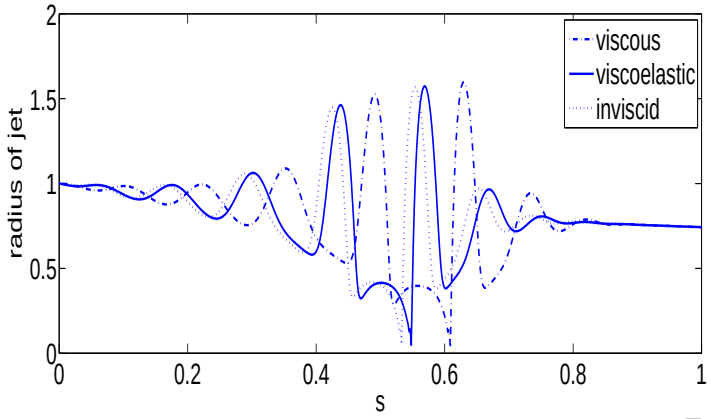

Figure 16: Graph showing the relationship between the radius of the jet and the arc-length for three different liquids. We notice that the break-up for non-Newtonian liquid jets (viscoelastic) happens faster than Newtonian liquid jets and after the inviscid liquid jets. We use $Re = 3000, We = 10, De = 20, k = 0.62, \alpha_s = 0.2$ and $Rb = 1$.

8. Conclusions

The Oldroyd-B model has been used to investigate the break-up of viscoelastic liquid curved jets. An asymptotic analysis has been used for deriving equations of motion at leading order. We found trajectories of liquid jets which emerged from an orifice are independent of the viscosity. The linear instability has been investigated to find the wavenumber of the most unstable mode and the growth rate for different values of the Rossby number (i.e. rotation rates), which shows that when rotation rates are high, the growth rate increases. From the linear instability, we have shown that viscoelastic jets are more unstable than Newtonian jets and less unstable than inviscid jets (which agrees with the finding of Goldin *et al.* [11]). A numerical method based on finite differences has been used to determine break-up lengths, droplet sizes and satellite sizes for viscoelastic curved jets. We can see that when the rotation rate is increased, the break-up length increases as well. This result also agrees with Newtonian liquid curved jets (Părău *et al.* [24]). In addition, when the viscosity rate is increased the break-up length increases. Satellite droplets also increase when the viscosity ratio is increased. Moreover, when the rotation rate is increased satellite droplets and main droplets are increase (see Fig. 12). We also found that viscoelastic jets break up before the Newtonian jets and after inviscid jets. The effect

of elasticity has been shown that when the Deborah number is increased the break-up length and the main droplets increase for viscoelastic liquid curved jets. Goldin *et al*. [11] have also shown for straight viscoelastic jets that the break-up length increases when viscoelasticity is increased. Finally, we have found that the break-up increased with increasing the viscosity ratio.

9. Acknowledgments

Abdullah Alsharif would like to thank Taif University for their financial support.

10. Appendix

The governing equations are

$$\epsilon n\frac{\partial u}{\partial s}+h_s\left(v+n\frac{\partial v}{\partial n}+\frac{\partial w}{\partial \phi}\right)+\epsilon n\left(v\cos\phi-w\sin\phi\right)\left(X_sZ_{ss}-Z_sX_{ss}\right)=0, \quad (47)$$

$$h_s\left(\epsilon\frac{\partial u}{\partial t}+\epsilon(v\cos\phi-w\sin\phi)(Z_{st}X_s-X_{st}Z_s)+v\frac{\partial u}{\partial n}+\frac{w}{n}\frac{\partial u}{\partial \phi}\right)+$$

$$\epsilon u\frac{\partial u}{\partial s}+\epsilon u(v\cos\phi-\sin\phi)(X_sZ_{ss}-Z_sX_{ss})=-\epsilon\frac{\partial p}{\partial s}+$$

$$\left(\frac{2\epsilon}{Rb}(v\cos\phi-\sin\phi)+\frac{\epsilon}{Rb^2}((X+r_0)X_s+ZZ_s)\right)h_s+$$

$$\frac{\alpha_s}{h_sRe}\left(\frac{-n\epsilon^3\cos\phi(X_sZ_{sss}-Z_sX_{sss})}{h_s^2}\left(\frac{\partial u}{\partial s}+v\cos\phi(X_sZ_{ss}-Z_sX_{ss})-\right.\right.$$

$$\left.w\sin\phi(X_sZ_{ss}-Z_sX_{ss})\right)+\frac{\epsilon^2}{h_s}\Big(-u(X_sZ_{ss}-Z_sX_{ss})^2+$$

$$\frac{\partial^2 u}{\partial s^2}+\left(2\frac{\partial v}{\partial s}\cos\phi+v\cos\phi\right)(X_sZ_{sss}-Z_sX_{sss})-w\sin\phi(X_sZ_{sss}-Z_sX_{sss})-$$

$$\left.2\frac{\partial w}{\partial s}\sin\phi(X_sZ_{ss}-Z_sX_{ss})\right)+(1+2\epsilon n\cos\phi(X_sZ_{ss}-Z_sX_{ss}))\frac{1}{n}\frac{\partial u}{\partial n}$$

$$\left.+nh_s\frac{\partial^2 u}{\partial n^2}+\frac{h_s}{n^2}\frac{\partial^2 u}{\partial \phi^2}-\frac{\epsilon}{n}\frac{\partial u}{\partial \phi}\sin\phi(X_sZ_{ss}-Z_sX_{ss})\right)+$$

$$\frac{1}{h_s\,Re}\bigg[\epsilon\frac{\partial T_{ss}}{\partial s}+2\epsilon(v\cos\phi-w\sin\phi)(X_sZ_{ss}-Z_sX_{ss})T_{ss}+$$

$$\frac{\partial T_{sn}}{\partial n}h_s+\frac{h_s}{n}\frac{\partial T_{s\phi}}{\partial\phi}+\frac{h_sv}{n}\,T_{s\phi}\bigg],\tag{48}$$

$$h_s\left(\epsilon\frac{\partial v}{\partial t}+\epsilon u\cos\phi(X_{st}Z_s-Z_{st}X_s)+v\frac{\partial v}{\partial n}+\frac{w}{n}\frac{\partial v}{\partial\phi}-\frac{w^2}{n}\right)+\epsilon u\frac{\partial v}{\partial s}-$$

$$\epsilon u^2\cos\phi(X_sZ_{ss}-X_{ss}Z_s)=-\frac{\partial p}{\partial n}h_s-\frac{2\epsilon h_s}{Rb}h_su\cos\phi+$$

$$\left(\frac{\epsilon}{Rb^2}\cos\phi((X+r_0)Z_s-ZX_s+n\cos\phi)\right)h_s+$$

$$\frac{\alpha_s}{h_sRe}\left(\frac{-\epsilon^3n\cos\phi(X_sZsss-X_{sss}Z_s)}{h_s^2}\left(\frac{\partial v}{\partial s}-u\cos\phi(X_sZ_{ss}-X_{ss}Z_s)\right)+\right.$$

$$\frac{\epsilon^2}{h_s}\bigg(-v\cos^2\phi\,(X_sZ_{ss}-X_{ss}Z_s)^2+\frac{\partial^2v}{\partial s^2}-2\frac{\partial u}{\partial s}\cos\phi\,(X_sZ_{ss}-X_{ss}Z_s)-$$

$$\left.u\cos\phi(X_sZsss-X_{sss}Z_s)+w\sin\phi\cos\phi(X_sZ_{ss}-X_{ss}Z_s)^2\right)+$$

$$(1+2\epsilon n\cos\phi(X_sZ_{ss}-X_{ss}Z_s))\,\frac{\partial v}{\partial n}+\,nh_s\frac{\partial^2v}{\partial n^2}-\epsilon(\frac{\partial v}{\partial\phi}-w)\sin\phi(X_sZ_{ss}-X_{ss}Z_s)+$$

$$\left.\frac{h_s}{n}(\frac{\partial^2v}{\partial\phi^2}-v-2\frac{\partial w}{\partial\phi})\right)+\frac{1}{h_sRe}\bigg[\epsilon\frac{\partial T_{sn}}{\partial s}+\epsilon(v\cos\phi-w\sin\phi)(X_sZ_{ss}-X_{ss}Z_s)\,T_{sn}-$$

$$\epsilon u\cos\phi T_{sn}+\frac{\partial T_{nn}}{\partial n}h_s+\frac{h_s}{n}\,\frac{\partial T_{n\phi}}{\partial\phi}+\frac{h_sv}{n}\,T_{n\phi}-\frac{w}{n}h_sT_{n\phi}\bigg],\tag{49}$$

$$h_s\left(\epsilon\frac{\partial w}{\partial t}+\epsilon u\sin\phi(Z_{st}X_s-X_{st}Z_s)+v\frac{\partial w}{\partial n}+\frac{w}{n}\frac{\partial w}{\partial\phi}-\frac{vw}{n}\right)+\epsilon u\frac{\partial w}{\partial s}+$$

$$\epsilon u^2\sin\phi(X_sZ_{ss}-X_{ss}Z_s)=\bigg(-\frac{1}{n}\frac{\partial p}{\partial\phi}h_s+\frac{2\epsilon}{Rb}u\sin\phi+$$

$$\frac{\epsilon}{Rb^2}\,\sin\phi(ZX_s-(X+r_0)Z_s-n\cos\phi)\Big)h_s+$$

$$\frac{\alpha_s}{h_s\,Re}\Bigg(\frac{-\epsilon^3 n\cos\phi(X_sZ_{sss}-X_{sss}Z_s)}{h_s^2}\Big(\frac{\partial w}{\partial s}+\,u\sin\phi(X_sZ_{ss}-X_{ss}Z_s)\Big)+$$

$$\frac{\epsilon^2}{h_s}\Bigg(-w\sin^2\phi\,(X_sZ_{ss}-X_{ss}Z_s)^2+\frac{\partial^2 w}{\partial s^2}+2\frac{\partial u}{\partial s}\sin\phi\,(X_sZ_{ss}-X_{ss}Z_s)+$$

$$u\sin\phi(X_sZ_{sss}-X_{sss}Z_s)+v\sin\phi\cos\phi(X_sZ_{ss}-X_{ss}Z_s)^2\Big)+$$

$$(1+2\epsilon n\cos\phi(X_sZ_{ss}-X_{ss}Z_s))\,\frac{\partial w}{\partial n}+\,nh_s\frac{\partial^2 w}{\partial n^2}-\epsilon(\frac{\partial w}{\partial\phi}+v)\sin\phi(X_sZ_{ss}-X_{ss}Z_s)+$$

$$\frac{h_s}{n}(\frac{\partial^2 w}{\partial\phi^2}-w+2\frac{\partial v}{\partial\phi})\Big)+\frac{1}{h_s\,Re}\Bigg[\epsilon\frac{\partial T_{s\phi}}{\partial s}+\epsilon(v\cos\phi-w\sin\phi)(X_sZ_{ss}-X_{ss}Z_s)\,T_{s\phi}-$$

$$\frac{\epsilon u}{h_s}T_{s\phi}\sin\phi(X_sZ_{ss}-X_{ss}Z_s)+\frac{\partial T_{n\phi}}{\partial n}h_s+\frac{h_s}{n}\frac{\partial T_{\phi\phi}}{\partial\phi}+\frac{2h_s v}{n}\,T_{\phi\phi}\Bigg]. \tag{50}$$

The equations of the extra stress tensor become

$$\frac{\partial T_{ss}}{\partial t}\,+\,\frac{u}{h_s}\frac{\partial T_{ss}}{\partial s}+\frac{v}{\epsilon}\frac{\partial T_{ss}}{\partial n}\,+\,\frac{w}{\epsilon n}\frac{\partial T_{ss}}{\partial\phi}\,-\,\frac{2}{h_s}\,\Big(\frac{\partial u}{\partial s}\,+v\,cos\phi\,\,-w\,\sin\,\phi\Big)$$

$$(X_sZ_{ss}-Z_sX_{ss})T_{ss}-\frac{2}{h_s}\Big(\frac{\partial v}{\partial s}+\frac{\partial u}{\partial n}\,-\,u\cos\,\phi\,(X_sZ_{ss}-Z_sX_{ss})\Big)\,T_{sn}-$$

$$\frac{2}{h_s}\,\Big(\frac{\partial w}{\partial s}\,+\frac{1}{n}\frac{\partial u}{\partial\phi}+u\,\sin\,\phi\,(X_sZ_{ss}-Z_sX_{ss})\Big)\,T_{s\phi}\,=$$

$$\frac{1}{De}\left[\frac{2(1-\alpha_s)}{h_s}\,\Big(\frac{\partial u}{\partial s}+(v\,\cos\,\phi-w\,\sin\,\phi)(X_sZ_{ss}-Z_sX_{ss})\Big)-T_{ss}\right] \tag{51}$$

$$\frac{\partial T_{sn}}{\partial t}+\frac{u}{h_s}\frac{\partial T_{sn}}{\partial s}+\frac{v}{\epsilon}\frac{\partial T_{sn}}{\partial n}\,+\,\frac{w}{\epsilon n}\frac{\partial T_{sn}}{\partial\phi}\,-\,\frac{1}{h_s}\,\Big(\frac{\partial u}{\partial s}\,+v\,cos\phi(X_sZ_{ss}-Z_sX_{ss})-$$

$$w\,\sin\,\phi(X_sZ_{ss}-Z_sX_{ss})\Big)T_{sn}-\frac{1}{h_s}\,\Big(\frac{\partial v}{\partial s}\,+\frac{\partial u}{\partial n}-\,u\,\cos\,\phi\,(X_sZ_{ss}-Z_sX_{ss})\Big)\,T_{nn}-$$

$$\frac{1}{\epsilon}\frac{\partial v}{\partial n}T_{sn}-\frac{1}{h_s}\,\Big(\frac{\partial w}{\partial s}\,+\frac{1}{n}\frac{\partial u}{\partial\phi}+\,u\,\sin\,\phi\,(X_sZ_{ss}-Z_sX_{ss})\Big)\,T_{n\phi}$$

$$-\Big(\frac{1}{\epsilon}\frac{\partial u}{\partial n}+\frac{1}{h_s}\frac{\partial v}{\partial s}-\frac{u}{h_s}\cos\,\phi\,(X_sZ_{ss}-Z_sX_{ss})\Big)T_{ss}-\Big(\frac{1}{\epsilon}\frac{\partial w}{\partial n}-\frac{w}{\epsilon n}+\frac{1}{\epsilon n}\frac{\partial v}{\partial \phi}\Big)T_{s\phi}$$
$$=\frac{1}{De}\left[\frac{(1-\alpha_s)}{h_s}\Big(\frac{\partial v}{\partial s}+\frac{h_s}{\epsilon}\frac{\partial u}{\partial n}-u\cos\phi(X_sZ_{ss}-Z_sX_{ss})\Big)-T_{sn}\right], \tag{52}$$

$$\frac{\partial T_{s\phi}}{\partial t}+\frac{u}{h_s}\frac{\partial T_{s\phi}}{\partial s}+\frac{v}{\epsilon}\frac{\partial T_{s\phi}}{\partial n}+\frac{w}{\epsilon n}\frac{\partial T_{s\phi}}{\partial \phi}-\frac{1}{h_s}\Big(\frac{\partial u}{\partial s}+v\,cos\phi(X_sZ_{ss}-Z_sX_{ss})-$$
$$w\,\sin\,\phi(X_sZ_{ss}-Z_sX_{ss})\Big)T_{sn}-\frac{1}{\epsilon}\left(\frac{\partial w}{\partial n}-\frac{w}{n}+\frac{1}{n}\frac{\partial v}{\partial \phi}\right)T_{s\phi}$$
$$-\Big(\frac{\partial u}{\epsilon\partial n}+\frac{1}{h_s}\frac{\partial v}{\partial s}-\frac{u}{h_s}\cos\,\phi\,(X_sZ_{ss}-Z_sX_{ss})\Big)T_{ss}-\frac{1}{h_s}\Big(\frac{\partial v}{\partial s}+\frac{\partial u}{\epsilon\partial n}-$$
$$u\,\cos\phi(X_sZ_{ss}-Z_sX_{ss})\Big)T_{nn}-\frac{1}{h_s}\Big(\frac{\partial w}{\partial s}+u\,\sin\phi(X_sZ_{ss}-Z_sX_{ss})+\frac{1}{\epsilon n}\frac{\partial u}{\partial \phi}\Big)T_{n\phi}$$
$$=\frac{1}{De}\left[(1-\alpha_s)\left(\frac{1}{\epsilon n}\frac{\partial u}{\partial \phi}+\frac{u}{h_s}\sin\phi(X_sZ_{ss}-Z_sX_{ss})+\frac{1}{h_s}\frac{\partial w}{\partial s}\right)-T_{s\phi}\right], \tag{53}$$

$$\frac{\partial T_{nn}}{\partial t}+\frac{u}{h_s}\frac{\partial T_{nn}}{\partial s}+\frac{v}{\epsilon}\frac{\partial T_{nn}}{\partial n}+\frac{w}{\epsilon n}\frac{\partial T_{nn}}{\partial \phi}$$
$$-2\Big(\frac{1}{\epsilon}\frac{\partial u}{\partial n}+\frac{1}{h_s}\frac{\partial v}{\partial s}-\frac{u}{h_s}\cos\,\phi\,(X_sZ_{ss}-Z_sX_{ss})\Big)T_{sn}-\frac{2}{\epsilon}\frac{\partial v}{\partial n}T_{nn}$$
$$-\frac{2}{\epsilon}\Big(\frac{\partial w}{\partial n}-\frac{w}{n}+\frac{1}{n}\frac{\partial v}{\partial \phi}\Big)T_{n\phi}=-\frac{1}{De}\left(\frac{2(1-\alpha_s)}{\epsilon}\frac{\partial v}{\partial n}-T_{nn}\right), \tag{54}$$

$$\frac{\partial T_{n\,\phi}}{\partial t}+\frac{u}{h_s}\frac{\partial T_{n\phi}}{\partial s}+\frac{v}{\epsilon}\frac{\partial T_{n\phi}}{\partial n}+\frac{w}{\epsilon n}\frac{\partial T_{n\phi}}{\partial \phi}$$
$$-\Big(\frac{1}{\epsilon}\frac{\partial u}{\partial n}+\frac{1}{h_s}\frac{\partial v}{\partial s}-\frac{u}{h_s}\cos\,\phi\,(X_sZ_{ss}-Z_sX_{ss})\Big)T_{s\phi}-\frac{1}{\epsilon}\Big(\frac{\partial v}{\partial n}+\frac{1}{n}\frac{\partial w}{\partial \phi}+\frac{v}{n}\Big)T_{n\phi}-$$
$$\frac{1}{\epsilon}\Big(\frac{\partial w}{\partial n}-\frac{1}{n}\frac{\partial v}{\partial \phi}\Big)T_{\phi\phi}-\Big(\frac{1}{\epsilon n}\frac{\partial u}{\partial \phi}+\frac{u}{h_s}\sin\,\phi\,(X_sZ_{ss}-Z_sX_{ss})+\frac{1}{h_s}\frac{\partial w}{\partial s}\Big)T_{sn}=$$
$$\frac{1}{De}\left[\frac{(1-\alpha_s)}{\epsilon}\Big(\frac{\partial w}{\partial n}-\frac{w}{n}+\frac{1}{n}\frac{\partial v}{\partial \phi}\Big)-T_{n\phi}\right], \tag{55}$$

$$\frac{\partial T_{\phi\phi}}{\partial t}+\frac{u}{h_s}\frac{\partial T_{\phi\phi}}{\partial s}+\frac{v}{\epsilon}\frac{\partial T_{\phi\phi}}{\partial n}+\frac{w}{\epsilon n}\frac{\partial T_{\phi\phi}}{\partial \phi}-\frac{2}{\epsilon n}\left(\frac{\partial v}{\partial \phi}-w+\frac{\partial w}{\partial n}\right)T_{n\phi}$$

$$-2\Big(\frac{1}{\epsilon n}\frac{\partial u}{\partial \phi}+\frac{u}{h_s}\sin\phi\,(X_sZ_{ss}-Z_sX_{ss})+\frac{1}{h_s}\frac{\partial w}{\partial \phi}\Big)T_{s\phi}-\frac{2}{\epsilon n}\left(\frac{\partial w}{\partial \phi}+v\right)T_{\phi\phi}=$$
$$\frac{1}{De}\left[\frac{2(1-\alpha_s)}{\epsilon n}\left(\frac{\partial w}{\partial \phi}+v\right)-T_{\phi\phi}\right], \qquad (56)$$

11. References

References

[1] Rayleigh, W. S., On the instability of jets, Proc. Lond. Math. Soc 10,4 (1878).

[2] Weber, C., Zum Zerfall eines Flussigkeitsstrahles. Z. Angew. Math. Mech, 11 (1931) 136-154.

[3] Papageorgiou, D. T., On the breakup of viscous liquid threads, Phys. Fluids, 7 (1995) 1529.

[4] Wallwork, I. M., Decent, S.P., King, A. C. and Schulkes, R. M. S., The trajectory and stability of a spiralling liquid jet. Part 1, Inviscid Theory, J. Fluid Mech., 459 (2002b)43-65.

[5] Decent, S. P., King, A. C. and Wallwork, I. M., Free jets spun from a prilling tower, Journal of Engineering Mathematics, 42 (2002) 265-282.

[6] Wallwork, I. M., The trajectory and stability of a spiralling liquid jet, Ph.D. Thesis, University of Birmingham, Birmingham (2002a).

[7] Decent, S. P., King, A. C., Simmons, M. H., Părău, E. I., Wong, D. C. Y., Wallwork, I. M., Gurney, C., and Uddin, J., The trajectory and stability of a spiralling liquid jet: Part II. Viscous Theory, Appl. Math. Modelling, 33 (12) (2007) 4283-4302.

[8] Uddin, J., Decent, S. P., and Simmons. M. J. H., The instability of shear thinning and shear thickening spiralling liquid jets: Linear theory. ASME J. of Fluids Eng., 128 (2006) 968975.

[9] Renardy, M., A numerical study of the asymptotic evolution and breakup of Newtonian and viscoelastic jets, J. Non-Newtonian Fluid Mech., 59 (1995) 267-282.

[10] Middleman, S., Stability of a viscoelastic jet, Chem. Eng. Sci. 20 (1965) 1037-1040.

[11] Goldin, M., Yerushalmi, J., Pfeffer, R., and Shinner, R., Breakup of a viscoelastic fluid. J. Fluid Mech. 38 (1969) 689-711.

[12] Magda, J. J., and Larson, R. G., 1988, A transition occurring in ideal elastic liquids during shear flow, J. Non-Newtonian Fluid Mech., 30 (1988) 1-19.

[13] Schummer, P., and Thelen, H. G., Break-up of a viscoelastic liquid jets, Rheol., Acta, 27 (1988) 39-43.

[14] Larson, R. G., Instabilities in viscoelastic flows, Rheol., Acta,31 (1992).

[15] Clasen, C., Eggers, J., Fonlelos, M. A., Li, j., and Mckinley, G. H., The beads-on-string structure of viscoelastic threads. J. Fluid Mech., 556 (2006) 283-308.

[16] Fontelos, M. A., Break-up and no break-up in a family for the evolution of viscoelastic jets, Z. angew. Math. Phys.,54 (2003) 84-111.

[17] Fontelos, M. A., and Li, J., On the evolution and rupture of filaments in Giesekus and FENE models, J. Non-Newtonian Fluid Mech., 118 (2004) 1-16.

[18] Davidson, M. R., Harvie, J. E., and Cooper-White, J. J., Simulation of pendant drop formation of a viscoelastic liquid, Korea-Australia Rheology Journal, 18 (2006) 41-49.

[19] Renardy, M., Stability of viscoelastic shear flows in the limit of high Weissenberg and Reynolds numbers, J. Non-Newtonian Fluid Mech., 155 (2008) 124-129.

[20] Liu, Z., and Liu, Z., Instability of a viscoelastic liquid jet with axisymmetric and asymmetric disturbance, International Journal of Multiphase Flow, 34 (2008) 42-60.

[21] Ardekani, A. M., Sharma, V., and McKinley, G. H., Dynamics of bead formation, filament thinning and breakup in weakly viscoelastic jets. J. Fluid Mech. (2010) 665, 46-56.

[22] Morrison, N. F., Harlen, O. G. 2010, Viscoelasticity in inkjet printing, Rheol., Acta, 49 (2010) 619-632.

[23] Uddin, J., An investigation into methods to control breakup and droplet formation in single and compound liquid jets. PhD thesis, University of Birmingham (2007).

[24] Părău, E. I., Decent, S. P., Simmons, M. J. H., Wong, D. C. Y. and King, A. C., Nonlinear viscous liquid jets from a rotating orifice, J. Of Eng. Maths., 57 (2007) 159-179.

[25] Wong, D. C. Y., Simmons, M. J. H., Decent, S. P., Parau, E. I. and King, A. C., Break-up dynamics and drop sizes distributions created from spiralling liquid jets, International Journal of Multiphase Flow, 30, 5 (2004) 499-520.

[26] Entov V. W. and Hinch, E. J., Effect of a spectrum of relaxation times on the capillary thinning of a filament of elastic liquid, J. Non-Newtonian Fluid Mech. 72 (1997), 31-53.

[27] Eggers, J., Nonlinear dynamics and breakup of free surface flows. Rev. Mod. Physis, 69, (3) (1997) 865-929.

[28] Hohman, M. M., Shin, M., Rutledge, G. abd Brenner, M. P., Electrospinning and electrically forced jets. II. Application. Phys. Fluids, 13, 8 (1984) 2221-2236.

[29] Părău, E. I., Decent, S. P., King, A. C., Simmons, M. J. H., Wong, D. C. Y., Nonlinear travelling waves on a spiralling liquid jet, Wave Motion, 43 (2006) 599-613.